

Bayesian estimation of pulsar parameters from gravitational wave data

Réjean J. Dupuis*

California Institute of Technology, Pasadena, CA 91125, USA and
University of Glasgow, Glasgow, G12 8QQ, UK

Graham Woan

University of Glasgow, Glasgow, G12 8QQ, UK

(Dated: August 2, 2018)

We present a method of searching for, and parameterizing, signals from known radio pulsars in data from interferometric gravitational wave detectors. This method has been applied to data from the LIGO and GEO 600 detectors to set upper limits on the gravitational wave emission from several radio pulsars. Here we discuss the nature of the signal and the performance of the technique on simulated data. We show how to perform a coherent multiple detector analysis and give some insight in the covariance between the signal parameters.

PACS numbers: 04.80.Nn, 02.50.-r

I. INTRODUCTION

Several kilometer-scale gravitational wave interferometers are now under construction or actively collecting data with unprecedented sensitivity [1, 2]. To make the best use of these data, sophisticated analysis methods have been developed to search for astrophysical signals that are doubtless buried in the noise. A promising class of sources of gravitational waves are rapidly rotating, and structurally asymmetric, neutron stars. Several mechanisms have been proposed that could support a varying quadrupolar mass distribution in these neutron stars, and the subsequent continuous emission of gravitational radiation [3, 4].

In this paper we present a detailed end-to-end description of an analysis technique which we have developed to infer the parameters of such sources using data from interferometric gravitational wave detectors [5]. Here we test the performance of the technique on simulated data. Whether a signal is clearly present or not, the method can be used to set upper limits on emission strength.

This method was successfully applied first to GEO 600 and LIGO data from their first science run (S1) to set upper limits on the strength of gravitational wave emission from pulsar J1939+2134 [6]. The search was modified and expanded to 28 isolated pulsars using data from LIGO's second science run (S2) [7]. This paper investigates the methods used in these two papers and sets performance benchmarks for the algorithm.

Searches for periodic gravitational wave signals from neutron stars are conventionally classed as *blind*, *directed* or *targeted*. A search is blind if no source parameters (such as sky position or spin evolution) are known a priori, so that the size of the parameter space to be explored is maximal. Blind searches represent a computationally demanding problem, and highly efficient analysis tech-

niques must be used [8, 9]. Even with these methods, a fully coherent search using many months of data is computationally intractable, and the size of the parameter space has the effect of decreasing the sensitivity of the search, as there is a good chance the noise will imitate a relatively strong source somewhere in the space [10]. Directed (known location) and targeted (known location and phase evolution) searches have smaller numbers of unknown parameters, and vastly smaller parameter spaces, making the detection level lower and increasing their sensitivity to gravitational waves.

Radio pulsars are particularly interesting class of targeted sources because i) we can monitor their rotation and make a very good guess at the gravitational waveform they produce and ii) their locations are known to high precision. In addition, the data pertaining to each pulsar can be restricted to a very narrow spectral window. Real interferometric data is usually contaminated by a large number of instrumental spectral lines, so the effects of these can be reduced significantly by analyzing only those narrow bands containing pulsar data.

This paper is structured as follows: section II describes the nature of the gravitational wave signal that we are expecting from pulsars. Section III describes how we filter and greatly reduce the size of the data set using a semi-standard heterodyne technique. In Section IV we present the Bayesian methodology used for this analysis and describe the two likelihood functions used in previous work. We demonstrate the performance of the algorithm on simulated data in Section V. Section VI concludes the paper with a brief summary.

II. NATURE OF GRAVITATIONAL WAVE SIGNAL

Here we summarize the form of gravitational waves emitted from a rotating rigid triaxial pulsar, described in detail in [11]. We take the special case of a triaxial ellipsoid rotating about its principal axis and therefore

*Electronic address: rejean@caltech.edu

emitting all its gravitational radiation at twice the rotation frequency. A freely precessing neutron star, with its spin and angular momentum axes non-aligned, would also emit at its rotation frequency but is expected to be strongly damped [12]. The regularity of signals from the majority of radio pulsars suggests that most of them are not precessing on a short timescales, if at all.

The gravitational wave amplitude from a triaxial neutron star seen from Earth is

$$h_0 = \frac{16\pi^2 G}{c^4} \frac{I_{zz} f_r^2}{r} \epsilon, \quad (1)$$

where r is the distance to the pulsar, I_{zz} its moment of inertia about the rotation (principal) axis, f_r the rotation frequency of the pulsar, and ϵ its equatorial ellipticity, defined in terms of its principal moments of inertia as

$$\epsilon = \frac{I_{xx} - I_{yy}}{I_{zz}}. \quad (2)$$

The gravitational wave strain on the detector will be frequency modulated, due to the relative motion of the Earth and the pulsar, and amplitude modulated by the antenna pattern of the interferometer. Following [8, 11], we can describe this measured signal as

$$h(t) = \frac{1}{2} F_+(t; \psi) h_0 (1 + \cos^2 \iota) \cos \Phi(t) + F_\times(t; \psi) h_0 \cos \iota \sin \Phi(t), \quad (3)$$

where F_+ and F_\times are the antenna responses to the $+$ and \times polarizations respectively, ψ is the polarization angle of the signal (determined by the position angle of the spin axis, projected on the sky), ι is the inclination of the pulsar with respect to the line-of-sight, and $\Phi(t)$ is the phase of the gravitational wave signal [23].

We choose to time the signal phase evolution $\Phi(T)$ with respect to the solar system barycenter (SSB), which is an inertial reference frame, so that to third-order in barycentric time, T ,

$$\Phi(T) = \phi_0 + 2\pi[f_s(T - T_0) + \frac{1}{2}\dot{f}_s(T - T_0)^2 + \frac{1}{6}\ddot{f}_s(T - T_0)^3], \quad (4)$$

where ϕ_0 is the phase of the signal at a fiducial time T_0 , f_s is the frequency of the signal ($= 2f_r$), \dot{f}_s is the first frequency derivative, and \ddot{f}_s is the second frequency derivative, all at time T_0 . The transformation between the barycentric time (T) and the topocentric time at the detector (t) is

$$T = t + \delta t = t + \Delta_{\text{Roemer}} + \Delta_{\text{Shapiro}} + \Delta_{\text{Einstein}} + \Delta_{\text{Binary}}, \quad (5)$$

where Δ_{Roemer} is the classical Roemer delay, $\Delta_{S\odot}$ is the Shapiro delay due to the curvature of space-time near the Sun, $\Delta_{E\odot}$ is the Einstein delay due to gravitational redshift and time dilation, and Δ_{Binary} contains corrections

related to the pulsar's orbit, which is zero for isolated neutron stars; see [13] for more details on these terms. However for pulsars in binary systems this term should include all the classical and relativistic corrections for the shifts in the time-of-arrival of the signal due to the motion of the source within the binary system. We will not consider binary pulsars in this analysis, but for more details on pulsar timing of binary systems see [14, 15] and references therein.

The second term in Equation 5, the Roemer delay, is the largest component (up to ~ 8.5 min) and due to the motion of the Earth within the solar system. In terms of the Earth's motion it is

$$\Delta_{\text{Roemer}} = \frac{\mathbf{r}_d \cdot \mathbf{k}}{c} + \frac{(\mathbf{r}_d \cdot \mathbf{k})^2 - |\mathbf{r}_d|^2}{2cd}, \quad (6)$$

where \mathbf{r}_d is the position of the detector with regard to the SSB, \mathbf{k} is a unit vector in the direction of the neutron star, c is the speed of light and d is the distance from the detector to the pulsar. In order to calculate the Roemer delay we need accurate knowledge of the position of the Earth with regard to the SSB. For our barycentering software [24] we use the solar system ephemerides published by the Jet Propulsion Laboratory [16]. The second term in Equation 6 is the timing parallax. This takes account of the curvature of the wavefronts emitted from the source and is only significant for the closest sources.

The Shapiro delay Δ_{Shapiro} is a relativistic correction for the curvature of space-time near the SSB. Since this curvature is not negligible there will be an extra time delay in the arrival of a signal. In principle this delay can be as large as $120 \mu\text{s}$ for signals passing near the edge of the Sun and therefore becomes important for the analysis of signals from millisecond pulsars over periods of ~ 1 yr. The maximum contribution from Jupiter however is only 200 ns and would not affect the sensitivity of a search.

The Einstein delay describes the combined effect of gravitational redshift and time dilation due to the motion of the Earth. This correction takes into account the varying gravitational potential experienced by a clock on the Earth as it follows its elliptical orbit around the Sun. Again this does not significantly affect signal searches.

III. THE COMPLEX HETERODYNE METHOD

Current ground-based interferometric detectors have broadband sensitivity to gravitational waves from frequencies of several tens of hertz up to several kilohertz. As a search for a continuous wave signal involves integrating for months or even years, the datasets involved can become very large indeed. However, the signal we are trying to extract in a targeted search is actually contained in only a very narrow frequency band, so accurate knowledge of the spin parameters of the source (from radio or X-ray observations) allows us to reduce the size of this data set considerably. To do this, we perform a complex heterodyne, followed by filtering and resampling

of the data, to reduce its size by a factor of about $\sim 10^6$ without loss of relevant information. Similar techniques have been applied in a wide range of optical, radio and gravitational searches for sinusoidal signals, most notably (in this context) [17].

We choose to perform a complex, slowly evolving, heterodyne on a targeted source to precisely unwind the apparent phase evolution of the source. However, for a signal from a pulsar recorded by an interferometric detector, there is still a time varying component remaining in the heterodyned signal from the antenna response pattern of the interferometer.

Since the source moves through the antenna pattern on a timescale that is much longer than the original periodic signal, after heterodyning we can re-sample the data with a much reduced sampling rate. In practice the new sampling rate is determined by our wish to monitor variations in the interferometer noise floor, which changes on timescales of minutes, hours, and days. Since we keep both the real and imaginary part of the sample for each minute, our effective bandwidth is 1/60 Hz centered on the heterodyning frequency which is the instantaneous frequency of the signal at the detector.

We take the calibrated output of a gravitational wave detector to be

$$s(t) = h(t) + n(t), \quad (7)$$

where $h(t)$ is a gravitational wave signal and $n(t)$ is noise that is stationary over some time period but not necessarily Gaussian. Using Equation 3 we recast the signal, $h(t)$, to

$$h(t) = A(t)e^{i\Phi(t)} + A^*(t)e^{-i\Phi(t)}, \quad (8)$$

where

$$A(t) = \frac{1}{4}F_+(t; \psi)h_0(1 + \cos^2 \iota) - \frac{i}{2}F_\times(t; \psi)h_0 \cos \iota, \quad (9)$$

and A^* is the complex conjugate of A . For a targeted pulsar we assume the frequency and frequency derivative terms are known from electromagnetic observations so that

$$\phi(t) = \Phi(t + \delta t) - \phi_0 \quad (10)$$

can be calculated to high precision. The heterodyning step involves multiplying the data from the interferometer by $e^{-i\phi(t)}$ to give

$$\begin{aligned} s_{\text{het}}(t) &= s(t)e^{-i\phi(t)} \\ &= A(t)e^{i\phi_0} + A^*(t)e^{-i\phi_0 - 2i\phi(t)} + n(t)e^{-i\phi(t)}. \end{aligned} \quad (11)$$

The heterodyning process removes the rotational phase evolution from the term in A , although this term will still vary over the day as the source moves through the antenna pattern of the interferometer. The second (upper sideband) term in A^* will oscillate at nearly twice the gravitational wave signal frequency.

We then apply a low-pass anti-aliasing filter to the heterodyned data stream prior to averaging. We note that, because the original time series was real, we lose no independent information by rejecting the upper sideband. We use a series of three third-order Infinite Impulse Response (IIR) Butterworth filters to do this, with frequency cut-offs that can be adjusted to the characteristics of the data. The main requirement is to prevent spectral disturbances from outside our final 1/60 Hz data band being aliased into our calculation of the averaged data. The selection of the IIR filters and the sampling rate ultimately depends on the opposing needs to over-resolve the timescales on which the noise is non-stationary and for a narrow band to avoid nearby spectral lines.

Finally we re-sample the filtered data to the post-filtering Nyquist rate and average the results (now s'_{het}) over a minute to form

$$B_k = \frac{1}{M} \sum_{i=1}^M s'_{\text{het}}(t_i), \quad (12)$$

where k is the minute index and M is the number of Nyquist samples in 1 minute (typically ~ 100).

In practice there are computational advantages to performing the heterodyning, filtering and re-sampling process described above in two steps, starting with a fixed heterodyning frequency and a filter that reduce the sampling rate to about 4 Hz. A second (variable) heterodyne can then be performed on the data to remove the Doppler shifts due to the motion of the Earth. The advantage is that the delay corrections between topocentric and barycentric time-of-arrival need only be calculated 4 times, rather than (for LIGO and GEO) 16384 times, per second.

With the high frequency term in Equation 11 suppressed we have

$$\begin{aligned} B_k &= \frac{1}{4}F_+(t_k; \psi)h_0(1 + \cos^2 \iota)e^{i\phi_0} \\ &\quad - \frac{i}{2}F_\times(t_k; \psi)h_0 \cos \iota e^{i\phi_0} + n(t_k)', \end{aligned} \quad (13)$$

where $n(t_k)'$ is the heterodyned and averaged complex noise in bin k . By the central limit theorem, we would expect the noise, $n(t_k)'$, to be well described by a Gaussian distribution, although the width of this distribution may change over time as the detector sensitivity evolves.

The heterodyned gravitational wave signal in this reduced data set depends on the same four unknown parameters in Equations 3 and 4: h_0 , ψ , ϕ_0 , and ι , which can be conveniently held as a vector, \mathbf{a} . We proceed in the next section by calculating the (Bayesian) probability of the data given these parameters and finally, through the application of Bayes' Theorem and marginalization, we obtain posterior probabilities for each of these parameters given the data collected.

IV. BAYESIAN FORMALISM

We take a straightforward Bayesian approach for the following analysis and calculate the posterior probability, $p(\mathbf{a}|\{B_k\}, I)$, of the pulsar parameters \mathbf{a} given the binned data, $\{B_k\}$. Bayes' Theorem tells us that

$$p(\mathbf{a}|\{B_k\}, I) = \frac{p(\mathbf{a}|I)p(\{B_k\}|\mathbf{a}, I)}{p(\{B_k\}|I)}, \quad (14)$$

where \mathbf{a} is the set of parameters inferred from data $\{B_k\}$, given our model I , and with likelihood $p(\{B_k\}|\mathbf{a}, I)$. I remains constant throughout the analysis, and will be dropped from the following expressions to avoid clutter. It should of course be noted that all the inferences we make from the data assume this model to be true. Note that the posterior probability distribution given here assumes that a signal is present in the data.

Our prior beliefs in the value of the parameters are held in $p(\mathbf{a})$ and we will use the least informative priors for most of the parameters over their respective ranges. A change in polarization angle of $\pi/2$ on the sky is equivalent to a change of signal sign (i.e., a change in signal phase, ϕ_0 , of π), so consistent priors are ϕ_0 uniform over $[0, 2\pi]$ and ψ uniform over $[-\pi/4, \pi/4]$. The prior probability density function for $\cos \iota$ is taken as uniform over $[-1, 1]$, corresponding to a uniform probability per unit solid angle for the orientation of the spin axis.

The prior probability for h_0 is more interesting. In principle the prior for h_0 should reflect all our initial beliefs on the gravitational wave strength, h_0 . If, for example we truly believe that gravitational wave emission is powered by the loss of kinetic energy from the pulsar (of known spindown rate), and that the moment of inertia of the pulsar is reasonably well constrained, then we should construct a prior that falls away sharply at strain levels which are above those consistent with this spindown upper limit. Of course we know that current detector sensitivities are insufficient to detect such a signal, and as a result the prior would overwhelm the broader likelihood function. We would learn nothing new from the experiment since the posterior probability distribution function (pdf) would largely resemble the prior pdf we chose.

At this stage in gravitational astronomy, a more useful statement would be concerned with what the observations told us that was *independent* of spindown arguments, and therefore the prior should reflect this greater sense of ignorance. We cannot exclude the prior possibility of $h_0 = 0$, so a fully scale-invariant Jeffreys prior ($\propto 1/h_0$) would not be appropriate. However, we are interested in being able to set conservative upper limits on the strength of any signals, and this argues in favour of using a uniform prior for h_0 . A uniform prior favours larger values of h_0 over smaller values (e.g., the prior probability for the range 0.1 to 1 is 10 times less than for 1 to 10), and represents, for most, an acceptable state of optimistic ignorance. The resulting upper limit for h_0 will therefore reflect the maximum value that could

reasonably be thought of as consistent with the data and has some additional merit because of that. In addition, a posterior based on a uniform prior for h_0 can be interpreted as a (marginal) likelihood for h_0 and more easily incorporated into future analyses with other data.

For further discussion choosing priors in cases, similar to this one, when the level of any signal may be below the sensitivity of the experiment, see [18]. Ultimately, if there is a strong detection the choice of the prior should not play an important role in the results since the likelihood function would be sufficiently strongly peaked to define the posterior. Conversely, if no signal is present at the sensitivity level of the instrument, the prior takes on a greater significance.

The full 4-dimensional posterior pdf contains all the information from our analysis but is difficult to interpret directly. It is therefore useful to reduce the dimensionality by marginalizing (integrating) over the less interesting (nuisance) parameters. The marginal distribution for one parameter can be viewed as a weighted average of all the distributions of this parameter given all the possible combinations of the other parameters. The parameter in which we are most interested is the gravitational wave amplitude h_0 , with a marginal pdf of

$$p(h_0|\{B_k\}) \propto \iiint p(\{B_k\}|\mathbf{a})p(\mathbf{a}) d\phi_0 d\psi d\cos \iota, \quad (15)$$

where the integral is performed numerically, over the full ranges of the nuisance parameters. The pdf for h_0 can then be normalised trivially.

Even without a detection, placing upper limits on h_0 can be physically interesting as we are essentially constraining the equatorial ellipticity of the neutron star. We define the upper limit of h_0 bounding 95% of the cumulative probability (from $h_0 = 0$) as the value h_{95} that satisfies

$$0.95 = \int_{h_0=0}^{h_{95}} p(h_0|\{B_k\})dh_0. \quad (16)$$

Note that such a limit can be placed on h_0 even if most of the probability is to be found some distance from $h_0 = 0$ and a strong signal is detected.

In order to calculate the likelihood function we need to have a model of the signal in the processed data. The model of the signal that we are searching for in the data set, $\{B_k\}$, is obtained by processing the original gravitational wave signal $h(t)$ in the same way that we processed the data to give

$$y(t_k; \mathbf{a}) = \frac{1}{4}F_+(t_k; \psi)h_0(1 + \cos^2 \iota)e^{i\phi_0} - \frac{i}{2}F_\times(t_k; \psi)h_0 \cos \iota e^{i\phi_0}. \quad (17)$$

We note that the model is complex and that the only time varying component is the antenna pattern of the interferometers. The Nyquist frequency for this signal is well below our reduced sampling rate of one B_k per

minute. In the following two sections we will present two different ways of evaluating the likelihood function depending on whether the variance of the data is known or unknown.

A. Gaussian model – known variance

Here we give the expression for the likelihood function assuming that we know, or can estimate accurately, the variance of the noise. We assume that the data comprises n samples of a signal, $y(t_k)$ (see Equation 17), embedded in complex Gaussian noise $N(0, \sigma_k)$ of zero mean and known overall variance σ_k^2 , so that

$$B_k = y_k + N(0, \sigma_k). \quad (18)$$

If the set of $\{B_k\}$ are independent, the likelihood of the data is simply the product of n bivariate normal distributions. Note that the distribution is bivariate because the data are now complex. The real and imaginary parts of the B_k 's have independent noise components, each with a variance $\sigma_k^2/2$. The likelihood of the parameters is therefore

$$p(\{B_k\}|\mathbf{a}, \{\sigma_k\}) = (\sqrt{2\pi}\sigma_k)^{-2n} \exp\left(-\sum_{k=1}^n \frac{|B_k - y_k|^2}{2\sigma_k^2}\right). \quad (19)$$

This Gaussian model for the likelihood was used for the first GEO 600 and LIGO analysis for signals from pulsar J1939+2134 [6]. For this analysis, the noise level σ_k was not known but was estimated for each B_k from the noise floor in a 4 Hz band of data around the signal frequency, assumed stationary for at least one minute. This gives 240×2 points contributing to the estimate of the variance, making the uncertainty in the point estimate of σ_k small enough to be ignored. The procedure is valid as long as the mean noise floor in the band is representative of the noise floor at the signal frequency, if there are no strong contaminating signals in the band and if the noise is sufficiently stationary. Although these requirements were largely met for [6], just one millisecond pulsar was involved in the study and they cannot be expected to be met in general. To address this an alternative model was developed for the S2 analysis [7].

B. Gaussian model – unknown variance

In the previous section we evaluated the likelihood function given the noise level, σ_k , for each B_k . Generally however, the noise level may not be known in advance or may not be well-estimated from the data. Here we described the likelihood function appropriate to this situation, which was used in the analysis of the LIGO S2 data [7].

If σ_k is estimated from a tighter bandwidth, or over a shorter period, fewer data contribute and the uncer-

tainty in its value may be too large to use a point estimate alone. Within our Bayesian framework the standard (and correct) approach is to treat the noise level as another nuisance parameter and marginalise over it, without computing a point estimate at all [19].

We begin by calculating the likelihood of a subset of m_j consecutive data points from $\{B_k\}$ which have a constant noise level σ_j . Once we have that expression, we will calculate the global likelihood simply using the product rule assuming that each segment of data is independent. We will again define n to be the total number of data points B_k and let M be the number of segments of data that we have assumed have the same noise level, so that

$$n = \sum_{j=1}^M m_j. \quad (20)$$

We can write the likelihood of the parameters, based on the j th subset of data and marginalised over σ_j as

$$\begin{aligned} p(\{B_k\}_j|\mathbf{a}) &\propto \int_0^\infty p(\{B_k\}_j, \sigma_j|\mathbf{a}) d\sigma_j \\ &\propto \int_0^\infty p(\sigma_j|\mathbf{a}) p(\{B_k\}_j|\mathbf{a}, \sigma_j) d\sigma_j, \end{aligned} \quad (21)$$

where $p(\sigma_j|\mathbf{a})$ is the prior for the noise floor and the likelihood $p(\sigma_j|\mathbf{a})p(\{B_k\}_j|\mathbf{a}, \sigma_j)$ is given by Equation 19. As σ_j is a non-zero scale parameter we take a Jeffreys prior, uniform in $\log \sigma_j$:

$$p(\sigma_j|\mathbf{a}) \propto \frac{1}{\sigma_j} \quad (\sigma_j > 0). \quad (22)$$

Our final conclusions would be essentially unchanged if a uniform prior was used instead of this Jeffreys prior [20]. Here we assume that the σ_j associated with each subset $\{B_k\}_j$ is constant over the m_j samples. In other words, we assume that the noise level of the interferometer, in a narrow frequency band around the gravitational wave signal, is stationary for this time. However, we allow the noise floor to change between each subset of data $\{B_k\}_j$. This allows us to dynamically track the noise floor seen in real interferometric data, which will inevitably vary on some timescale, as the instrumental performance varies. The length of the j th subset, over the which the data is assumed stationary, can also be adjusted to reflect the known timescale of these variations.

Using Equations 19, 21 and 22, the likelihood of the parameters based on a subset $\{B_k\}_j$ of constant noise σ_j is

$$p(\{B_k\}_j|\mathbf{a}) \propto \int_0^\infty \frac{1}{\sigma_j^{2m_j+1}} \exp\left(-\sum_{k=k_1(j)}^{k_2(j)} \frac{|B_k - y_k|^2}{2\sigma_j^2}\right) d\sigma_j \quad (23)$$

where $m_j = k_2(j) - k_1(j) + 1$. This reduces to

$$p(\{B_k\}_j|\mathbf{a}) \propto \left(\sum_{k=k_1(j)}^{k_2(j)} |B_k - y_k|^2\right)^{-m_j}, \quad (24)$$

which is equivalent to a Student's t -distribution with $2m_j - 1$ degrees of freedom. Recall that the likelihood derived in Equation 24 is for a set of m_j data points B_k with the same σ_j . The joint likelihood of all the M stretches of data, taken as independent, is therefore

$$p(\{B_k\}|\mathbf{a}) \propto \prod_j^M \left(\sum_{k=k_1(j)}^{k_2(j)} |B_k - y_k|^2 \right)^{-m_j}. \quad (25)$$

We note that there is (of course) no explicit reference to the noise level, but the lengths of the stationary intervals, m_j , can be adjusted to reflect the performance of the detectors.

V. PERFORMANCE ON SIMULATED DATA

A. Expected sensitivity

The analysis described above is optimal (in a Bayesian sense) for the data available from one or more science runs. It is however instructive to examine the long-term performance of the method on a large series of simulated data sets, both to confirm that the average performance complies with our expectations and to ease comparisons with methods based on sampling theory.

To do this, we calculated the h_{95} upper limits from 4000 simulated data sets, of length 10 days, varying the location of the putative source in the sky and the location of the detector in each set. The locations of the sources were picked randomly from a uniform distribution over the sky, and the detector locations were the GEO 600 and the two LIGO sites.

From these we can express the average 95% upper limit $\langle h_{95} \rangle$ as a function of observation time T and single-sided noise power spectral density, $S_n(f)$. Empirically, from these simulations,

$$\langle h_{95} \rangle = (10.8 \pm 0.2) \sqrt{S_n(f)/T}, \quad (26)$$

where the range accounts for the location of the detector. Figure 1 shows the distribution of h_{95} that contributed to this, for $S_n(f)/T = 1$. Note that the width and skew of the distribution are relatively large, so the actual upper limit from an observing run could reasonably be up to a factor of two larger than $\langle h_{95} \rangle$.

B. Combining data from a network of detectors

Several gravitational wave detectors are currently collecting data, and ideally we should be able to use the observations from all detectors in a coherent manner in order to draw the best possible inference about the source parameters. In a Bayesian analysis all observations enter via the likelihood function. Assuming that the noise from each interferometer is independent, by the product rule

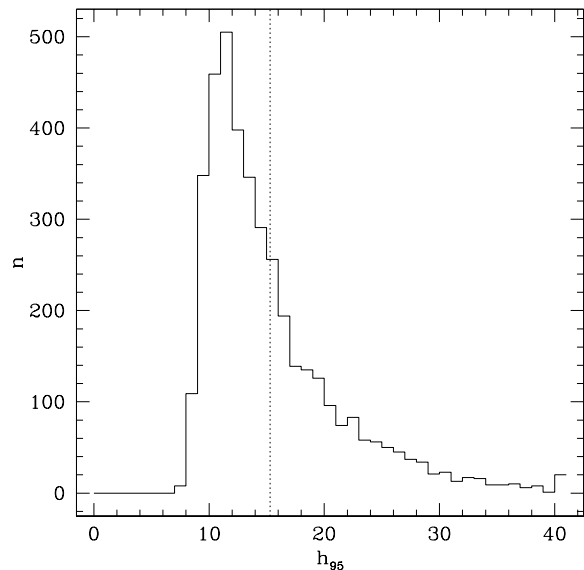


FIG. 1: Distribution of 95% upper limits on h_0 for 4000 simulations, using sources randomly located on the sky with $S_n(f)/T = 1$.

the global likelihood is simply the product of the individual likelihoods. For example, by combining observations from GEO 600 and the three LIGO interferometers, we would get

$$p(\{B_k\}_{\text{Joint}}|\mathbf{a}) = \prod_{i=1}^4 p(\{B_k\}_i|\mathbf{a}, i) \quad (27)$$

where the product is over the 4 km Hanford interferometer (H1), the 2 km Hanford interferometer (H2), the 4 km Livingston interferometer (L1), and GEO 600.

This likelihood contains all the information on the source parameters that is contained in the data, optimally combining the data from all the interferometers in a coherent way. Note that the observation periods can be different and so can the sensitivity of the detectors, although for detectors with very different sensitivities, this will closely approximate the likelihood based on just the most sensitive instrument.

For illustration, we generated four sets of data of 10 days length with Gaussian noise ($\mu = 0$ and $\sigma = 1$) as if from GEO 600 and the three LIGO interferometers. As these IFOs are modelled as having the same sensitivity, we would expect the coherent results to be approximately $\sqrt{4}$ times tighter than the individual results (distinguished from a factor of four increase in observing time only by the differing antenna patterns of the instruments). The four posterior pdfs for each detector as well as the joint multi-detector posterior pdf for h_0 are shown in Figure 2. The individual 95% upper limits are 0.15 for GEO 600, 0.16 for H1, 0.18 for H2, and 0.13 for L1 giving an average of 0.155. The combined 95%

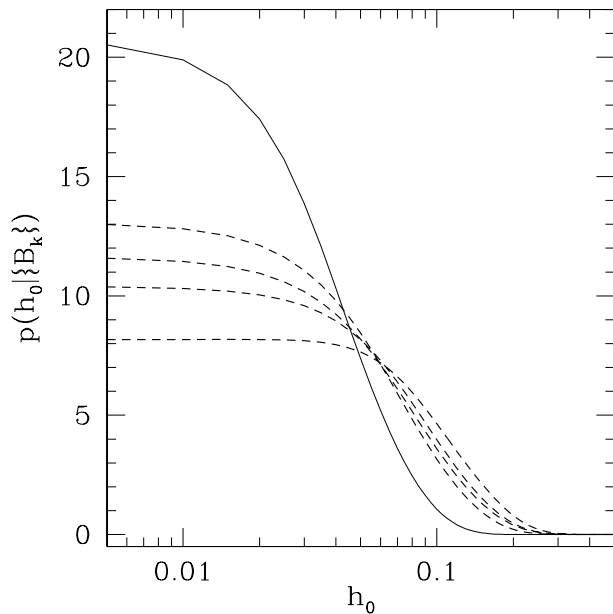


FIG. 2: Multi-detector posterior pdfs with simulated data. The solid line represents the joint marginalised posterior pdf for h_0 using the data from four separate interferometers. The dashed lines are the corresponding pdfs from the individual detectors.

upper limit, on the other hand, is 0.08, which is indeed approximately a factor of 2 better than the average of the limits from the individual detectors. This technique was first applied to real gravitational wave data in [7]. The equivalent multi-detector analysis using the \mathcal{F} -statistic method [8] has recently been developed by Cutler and Schutz [21].

It is important to realise that the posterior curve derived from a particular observation represents a probabilistic statement about the value of h_0 based on the data in hand and may, if we are unlucky, be wildly at odds with the truth. As a result the upper limit derived from one instrument alone will occasionally be lower than that from the coherent combination of instruments.

C. Effects of changing the noise level

The widths of the marginal posteriors depend on both the level of the noise and the covariance of the parameters. Here we demonstrate the noise dependence by analysing three sets of data with different, sometimes modulated, noise variances. Each data set corresponds to 10 days of observations. The first contains Gaussian noise with $\mu = 0$ and $\sigma = 1$. For the second data set, the noise level alternates each 30 minutes between $\sigma = 10$ and $\sigma = \frac{1}{2\sqrt{2}}$. For the third data set, the noise level alternates each 30 minutes between $\sigma = 100$ and $\sigma = \frac{1}{5\sqrt{2}}$. Two time series plots showing representative stretches of

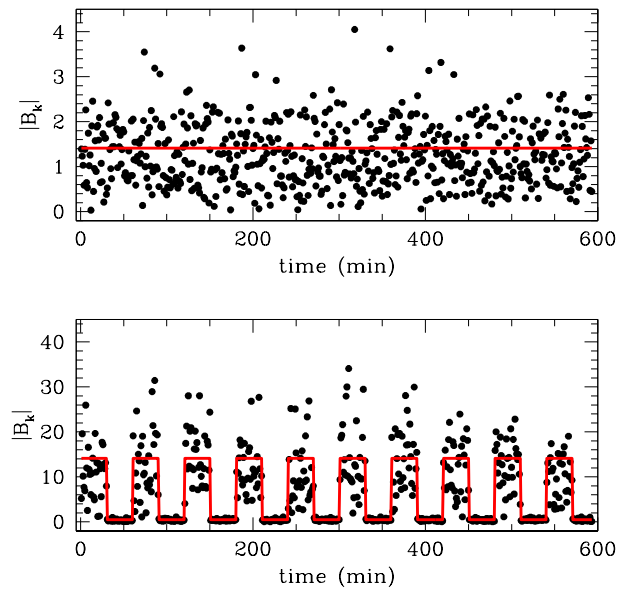


FIG. 3: Time series of B_k showing the effect of a changing noise level. The dots are the $|B_k|$ and the line represents the variance of the B_k 's. The top figure represents the first data set with constant variance and the bottom figure represents the second data set with alternating variance.

data from the first and second sets are shown Figure 3.

For this test, we repeated and averaged the posterior pdfs for 100 generations of the data sets described above. The average marginalised posterior pdfs for h_0 are shown in Figure 4. Using the 66% upper limit on h_0 to characterise the width of the pdfs we have $h_0 < 0.095$ for case 1, $h_0 < 0.047$ for case 2, and $h_0 < 0.019$ for case 3. The second posterior is narrower than the first by a factor of 2.02 and the third by a factor of 5.05. For no signal, these results are roughly what we would expect: in the two cases with alternating noise levels, about half of the data has very low sensitivity compared to the other half, and we can assume this noisy half does not play a significant part in the posterior. Therefore these cases are approximately equivalent to a continuous observation at the greater sensitivity level but for half the full observing period, and the reduced time lowers the sensitivity by $\sqrt{2}$. Thus compared to the first case with constant noise, we would expect the two sets with alternating noise levels to have widths which are narrower by factors of about 2 and 5, which is what we see.

D. Covariance between parameters

To illustrate the covariance between the signal parameters we generated a 10 days time series containing a signal with the following parameters and Gaussian noise of unit variance: $h_0 = 0.25$, $\cos \iota = 0.1$, $\phi_0 = 180^\circ$, $\psi = 0.0^\circ$. It is clear from the emission model that if $\cos \iota \neq 0$, h_0 and $\cos \iota$ are strongly anti-correlated, as are ψ and ϕ_0 . The

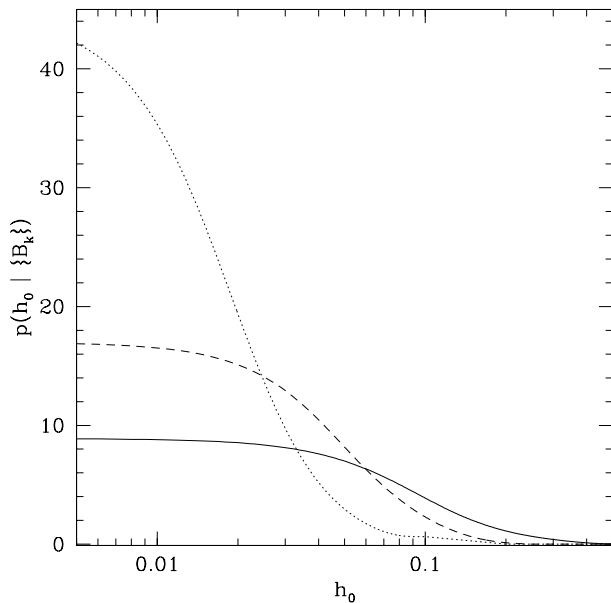


FIG. 4: Averaged marginalised posterior pdfs for h_0 for three scenarios: constant unit variance (solid line), alternating noise level between $\sigma = 10$ and $\sigma = \frac{1}{2\sqrt{2}}$ (dashed line), and alternating noise level between $\sigma = 100$ and $\sigma = \frac{1}{5\sqrt{2}}$ (dotted line).

correlation can be seen clearly in the probability density contour plots in Figure 5. The covariance between $\cos \iota$ and h_0 contributes strongly to the overall width of the marginal pdf of h_0 , making the precise value of h_0 somewhat difficult to determine even under conditions of relatively high signal-to-noise ratio. The correlation between h_0 and $\cos \iota$ is also visible when no gravitational wave signal is injected in the data ($h_0 = 0$), largely because of our choice of a uniform prior for h_0 which holds out high hopes for a strong signal in the data (Figure 6). When no such signal is seen, this is interpreted as an indication that the pulsar is oriented unfavorably and the posterior probability slightly increases around $\cos \iota = 1$, where only the ‘+’ polarization is present.

VI. CONCLUSIONS

In this paper we have presented an end-to-end Bayesian method of searching for, and parameterizing, gravitational waves from known pulsars. The method involves processing the raw data to reduce the number of samples required for the analysis. We calculated the likelihood function for given model parameters from the decimated data, so reducing computational requirements. The algorithm has been validated by retrieving the correct signal parameters from simulated data. We have also shown that it is easily adapted to deal with a network of detectors.

This methodology was initially developed for targeted

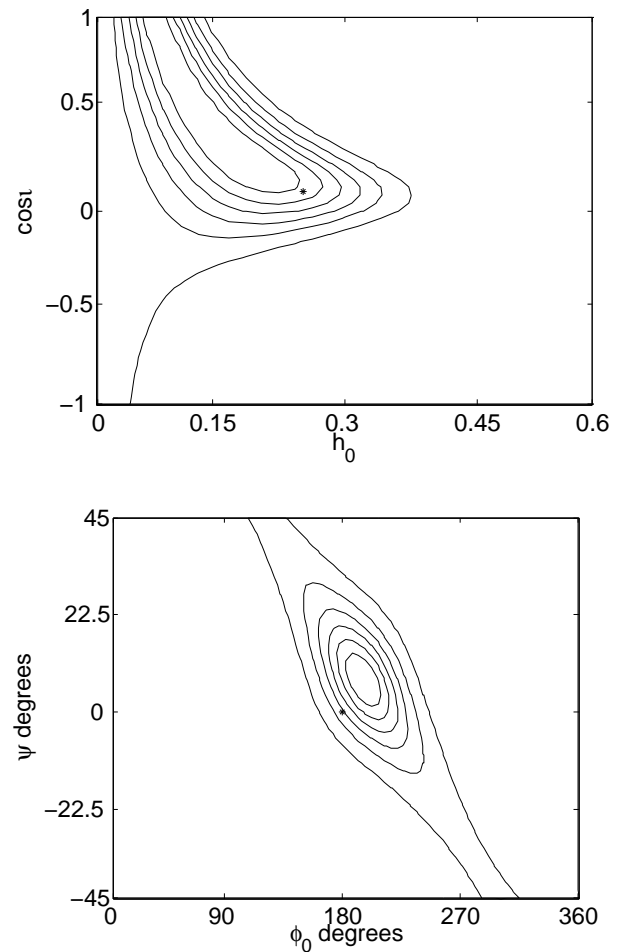


FIG. 5: Equally-spaced contours of constant probability density for (top) the joint posterior probability of $\cos \iota$ and h_0 and (bottom) ψ and ϕ_0 . The marker indicates the location of the simulated signal.

searches with known locations and spin evolutions of the sources. Further work has now been done studying the feasibility of expanding the numbers of parameters by taking advantage of Monte Carlo Markov Chain (MCMC) techniques [22]. These techniques are required when the number of unknown parameters is significantly increased, when the method presented here would be too computationally intensive. In a future paper we will address how this method has been adapted to search for gravitational emission from pulsars in binary systems. The algorithm presented in this paper, with the binary modification, is currently being applied to GEO 600 and LIGO data from the S3 and S4 science runs.

Acknowledgments

The authors would like to thank the LSC Pulsar Group for useful discussions. This work was supported by

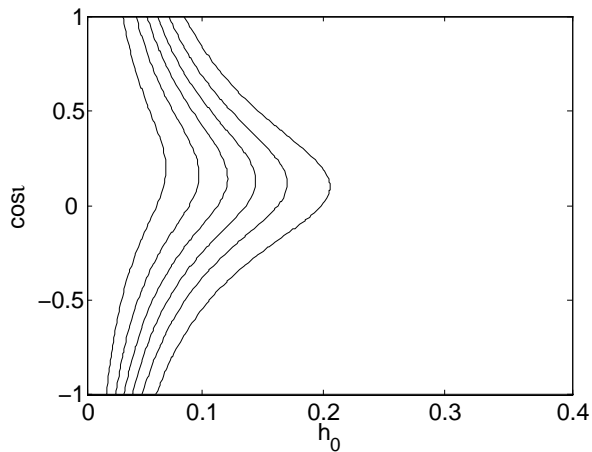


FIG. 6: Equally-spaced contours of constant probability, showing the covariance between h_0 and $\cos i$, for Gaussian noise with no signal but a uniform prior for h_0 .

the Natural Sciences and Engineering Research Council of Canada, Universities UK, and the University of Glasgow. RJD would also like to acknowledge funding from the National Science Foundation. This document has been assigned LIGO Laboratory document number LIGO-P050046-00-Z.

-
- [1] B. Abbott *et al.* (LIGO Scientific Collaboration), Nuclear Instruments and Methods in Physics Research A **517**, 154 (2004).
- [2] B. Caron *et al.* (VIRGO Collaboration), Nuclear Physics B Proceedings Supplements **54**, 167 (1997).
- [3] C. Cutler, Phys. Rev. D **66**, 084025 (2002).
- [4] B. Owen, astro-ph/0503399 (2005).
- [5] R. J. Dupuis, Ph.D. thesis, University of Glasgow (2004).
- [6] B. Abbott *et al.* (LIGO Scientific Collaboration), Phys. Rev. D **69**, 082004 (2004).
- [7] B. Abbott *et al.* (LIGO Scientific Collaboration), Physical Review Letters **94**, 181103 (2005).
- [8] P. Jaranowski, A. Królak, and B. F. Schutz, Phys. Rev. D **58**, 063001 (1998).
- [9] B. Krishnan, A. M. Sintes, M. A. Papa, B. F. Schutz, S. Frasca, and C. Palomba, Phys. Rev. D **70**, 082001 (2004).
- [10] P. R. Brady, T. Creighton, C. Cutler, and B. F. Schutz, Phys. Rev. D **57**, 2101 (1998).
- [11] M. Zimmermann and E. Szedenits, Phys. Rev. D **20**, 351 (1979).
- [12] D. I. Jones and N. Andersson, MNRAS **331**, 203 (2002).
- [13] D. C. Backer and R. W. Hellings, Annu. Rev. Astron. Astrophys. **24**, 537 (1986).
- [14] J. H. Taylor and J. M. Weisberg, Astrophys. J. **345**, 434 (1989).
- [15] J. M. Weisberg and J. H. Taylor, ArXiv Astrophysics e-prints (2004), arXiv:astro-ph/0407149.
- [16] <http://ssd.jpl.nasa.gov/horizons.html>.
- [17] T. M. Niebauer, A. Rudiger, R. Schilling, L. Schnupp, W. Winkler, and K. Danzmann, Phys. Rev. D **47**, 3106 (1993).
- [18] G. D'Agostini, ArXiv Physics e-prints (physics/9906048, 1999).
- [19] G. L. Bretthorst, *Bayesian spectrum analysis and parameter estimation - Lecture Notes in Statistics Vol 48* (Springer-Verlag, Berlin, 1988).
- [20] D. Sivia, *Data analysis: A Bayesian tutorial* (Oxford University Press, 1996).
- [21] C. Cutler and B. F. Schutz, ArXiv General Relativity and Quantum Cosmology e-prints (2005), arXiv:gr-qc/0504011.
- [22] N. Christensen, R. J. Dupuis, G. Woan, and R. Meyer, Phys. Rev. D **70**, 022001 (2004).
- [23] Authors do not agree on whether one should work in terms of signal phase or rotational phase in these expressions. We use the convention of [6] and [7], so that $\Phi = \Phi_{\text{sig}} = 2\Phi_{\text{rot}}$.
- [24] The timing routines that we used are available in the LIGO Analysis Library available at <http://www.lsc-group.phys.uwm.edu/daswg/projects/lal.html>